Redox Behavior of Ferrocene Derivatives. 2.[1] Bis(η^5-tricyclo[5.2.1.$0^{2,6}$]deca-2,5,8-trien-6-yl)iron and Related Molecules

Judith C. Gallucci,[2a,3] Giuliana Opromolla,[2c] Leo A. Paquette,*[,2a] Luca Pardi,[2b] Paulo F. T. Schirch,[2a] Mark R. Sivik,[2a] and Piero Zanello*[,2c]

Evans Chemical Laboratories, The Ohio State University, Columbus, Ohio 43210, Dipartimento di Chimica dell'Università di Firenze, Via Maragliano 77, 50144 Firenze, Italy, and Dipartimento di Chimica dell'Università di Siena, Pian dei Mantellini 44, 53100 Siena, Italy

Received October 1, 1992

The series of ferrocene-like derivatives **5–11**, in which the cyclopentadienyl rings are fused to bicyclic norbornane- or pinane-like fragments, has been studied electrochemically in order to test the ability of these derivatives to lose one electron as well as to quantify any stereoelectronic effects associated with coordination of the bicyclic moieties above or below the plane of the cyclopentadienyl rings. The X-ray structure of the cation bis(η^5-tricyclo[5.2.1.$0^{2,6}$]deca-2,5,8-trien-6-yl)iron(III) ([**5**]$^+$, as its TCNQ salt) has been determined, thus allowing us to evaluate the stereochemical reorganizations accompanying one-electron removal from the corresponding neutral iron(II) congener (**5**). The EPR spectra of all the electrogenerated cations [**5**]$^+$–[**11**]$^+$ have been recorded at liquid-helium temperature.

Introduction

The fusion of a cyclopentadiene ring to a bicyclic framework as in **1–4** provides for π-facial discrimination during the complexation of their anions to metals. The distinctive stereochemical facets of these reactions have been elucidated,[4-7] and more recently, the relationship of the exo/endo product ratios to the state of aggregation and relative orientation of the lithium counterion has been defined.[8]

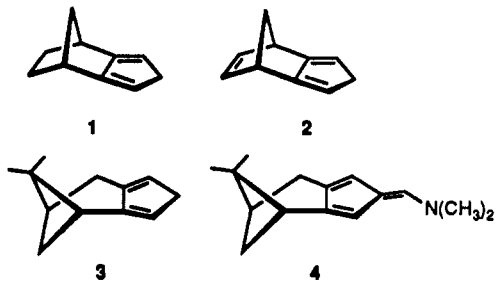

Stereoelectronic effects present in the associated cyclopentadienide anions[4,9] can reasonably be expected to persist in their metallocene derivatives. In the present work, a detailed electrochemical study of the ferrocene-like complexes **5–12** has been undertaken for the purpose of quantifying the differences

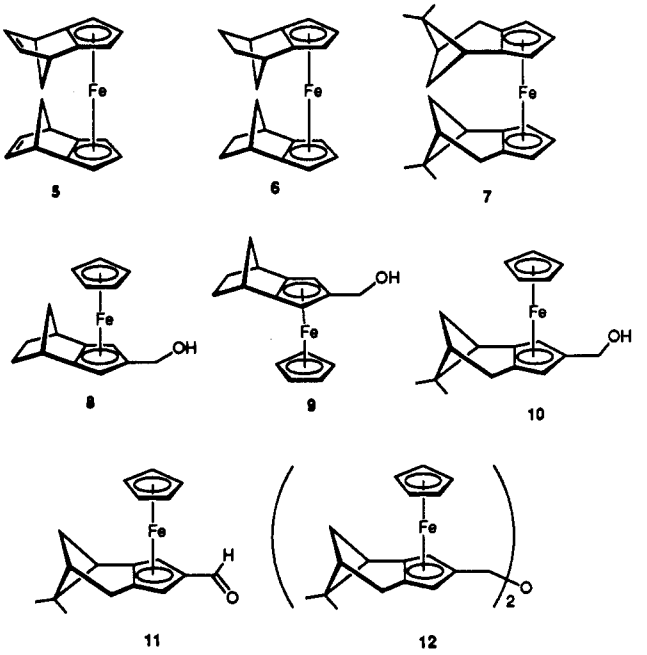

associated with above- and below-plane coordination. As expected, the mononuclear complexes **5–11** undergo reversible one-electron oxidation, whereas the dinuclear complex **12** undergoes two almost overlapping one-electron removals. The stereodynamic aspects of these redox changes have also been considered and realized for the **5**/[**5**]$^+$ couple by comparison of their X-ray crystallographic structures. Among the hundreds of known mononuclear ferrocenes, the only ferrocene–ferrocenium couples known to us to have been crystallographically characterized previously are $Fe(C_5H_5)_2/[Fe(C_5H_5)_2]^+$,[10,11] 1,1′,2,2′,4,4′-tris(trimethylene)ferrocene/1,1′,2,2′,4,4′-tris(trimethylene)ferrocenium,[12,13] $Fe(C_5Me_4H)_2/[Fe(C_5Me_4H)_2]^+$,[14,15] $Fe(C_5Me_5)_2/[Fe(C_5Me_5)_2]^+$,[16,17] and $Fe(C_5Bz_5)_2/[Fe(C_5Bz_5)_2]^+$.[18,19]

(1) Part 3: Zanello, P.; Opromolla, G.; Pardi, L.; Pannell, K. H.; Sharma, H. K. *J. Organomet. Chem.*, in press.
(2) (a) The Ohio State University. (b) Dipartimento di Chimica dell'Università di Firenze. (c) Dipartimento di Chimica dell'Università di Siena.
(3) Author to whom inquiries relating to the X-ray crystallographic analysis should be addressed.
(4) Hsu, L.-Y.; Hathaway, S. J.; Paquette, L. A. *Tetrahedron Lett.* **1984**, 259.
(5) Paquette, L. A.; Schirch, P. F. T.; Hathaway, S. J.; Hsu, L.-Y.; Gallucci, J. C. *Organometallics* **1986**, *5*, 490.
(6) Paquette, L. A.; McKinney, J. A.; McLaughlin, M. L.; Rheingold, A. L. *Tetrahedron Lett.* **1986**, *27*, 5599.
(7) Paquette, L. A.; Gugelchuk, M.; McLaughlin, M. L. *J. Org. Chem.* **1987**, *52*, 4732.
(8) (a) Paquette, L. A.; Bauer, W.; Sivik, M. R.; Buhl, M.; Feigel, M.; Schleyer, P. v. *J. Am. Chem. Soc.* **1990**, *112*, 8776. (b) Bauer, W.; O'Doherty, G. A.; Schleyer, P. v. *J. Am. Chem. Soc.* **1991**, *113*, 7093. (c) Bauer, W.; Sivik, M. R.; Friedrich, D.; Schleyer, P. v.; Paquette, L. A. *Organometallics*, in press.
(9) (a) Paquette, L. A.; Charumilind, P.; Gallucci, J. C. *J. Am. Chem. Soc.* **1983**, *105*, 7364. (b) Paquette, L. A. In *Stereochemistry and Reactivity of π Systems*, Watson, W. H., Ed.; Verlag Chemie: Deerfield Beach, FL, 1983, pp 41–73.
(10) Seiler, P.; Dunitz, J. D. *Acta Crystallogr.* **1979**, *B35*, 1068.
(11) Martinez, R. Tiripicchio, A. *Acta Crystallogr.* **1990**, *C46*, 202 and references therein.
(12) Hillman, M.; Fujita, E. *J. Organomet. Chem.* **1978**, *155*, 87.
(13) Hillman, M.; Larson, A. C. *J. Organomet. Chem.* **1985**, *280*, 389.
(14) Schmitz, D.; Fleischhauer, J.; Meier, U.; Schleker, W.; Schmitt, G. *J. Organomet. Chem.* **1981**, *205*, 381.
(15) Miller, J. S.; Glatzhofer, D. T.; O'Hare, D. M.; Reiff, W. M.; Chakraborty, A.; Epstein, A. J. *Inorg. Chem.* **1989**, *28*, 2930.

0020-1669/93/1332-2292$04.00/0

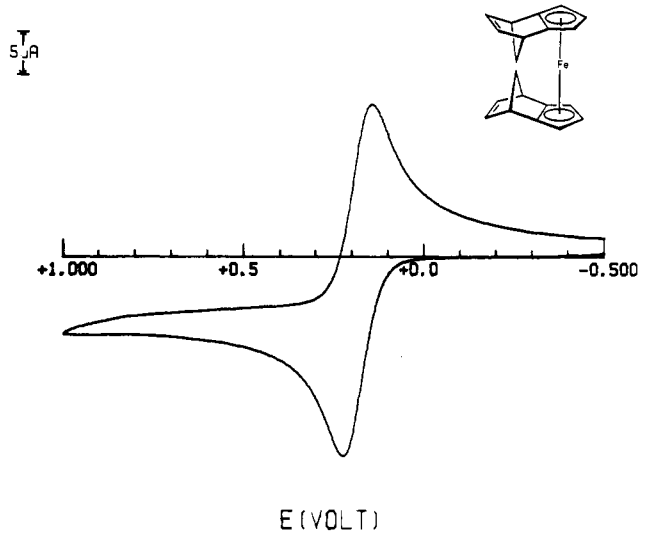

Figure 1. Cyclic voltammogram recorded at a platinum electrode on a CH_2Cl_2 solution containing **5** (2.0×10^{-3} mol dm^{-3}) and $[NBu_4][PF_6]$ (0.2 mol dm^{-3}). Scan rate: 0.05 V s^{-1}.

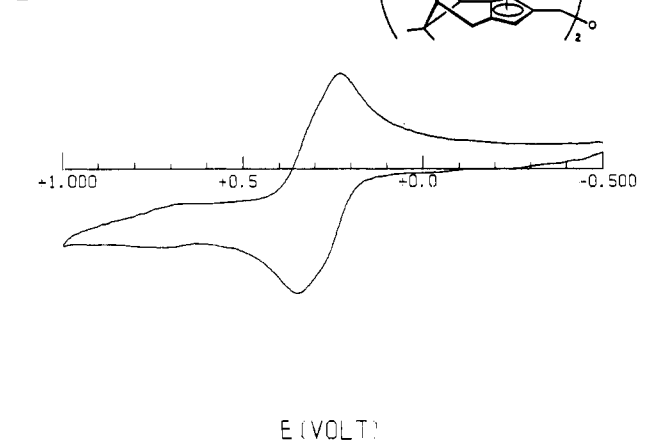

Figure 2. Cyclic voltammogram recorded at a platinum electrode on a CH_2Cl_2 solution containing **12** (2.0×10^{-4} mol dm^{-3}) and $[NBu_4][PF_6]$ (0.2 mol dm^{-3}). Scan rate: 0.05 V s^{-1}.

Results and Discussion

Electrochemistry. Figure 1 shows the cyclic voltammetric response exhibited by **5** in dichloromethane solution. Controlled potential coulometry ($E_w = +0.5$ V) shows that the anodic process involves the consumption of one electron/molecule. The deep-green solution resulting from exhaustive oxidation of the original lemon yellow solution displays a cyclic voltammogram quite complementary to that shown in Figure 1. This datum points out the chemical reversibility of the **5**/[**5**]$^+$ redox transformation.

Analysis[20] of the cyclic voltammetric response with scan rates varied from 0.02 to 10.24 V s^{-1} showed that (i) the i_{pc}/i_{pa} current ratio is constantly equal to 1, (ii) the current function $i_{pa}/V^{1/2}$ remains substantially constant, and (iii) the peak-to-peak separation, ΔE_p, progressively increases from 72 to 392 mV. In view of the verified chemical reversibility of the oxidation process, the trend of ΔE_p with scan rate warranted further consideration. The extent of electrochemical reversibility is recognized to be roughly related to the extent of stereochemical reorganization accompanying the electron transfer.[21] Although an electrochemically reversible one-electron step is expected to exhibit a constant ΔE_p value of 59 mV independent of scan rate,[20] uncompensated solution resistances may be responsible for the significant departure observed at high scan rates. Consequently, the most reliable data are presumed to reside in those measurements recorded at low scan rates. In this light, the **5**/[**5**]$^+$ redox change does not seem to be accompanied by significant structural reorganization.

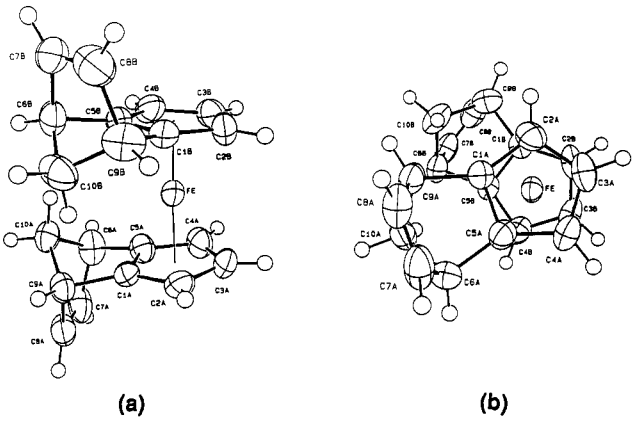

Figure 3. ORTEP plots of the side view (a) and top view (b) of the final X-ray model of **5**·2TCNQ. The non-hydrogen atoms are represented by 50% probability thermal ellipsoids. The hydrogen atoms are drawn with an artificial radius.

Table I. Formal Electrode Potentials (in V vs SCE) and Peak-to-Peak Separation (in mV, at 0.1 V s^{-1}) for the Oxidation of the Mononuclear Complexes **5**–**11** and Related Ferrocene Molecules in Dichloromethane Solution

complex	$E^\circ_{(0/+)}$	ΔE_p
5	+0.19	82
6	+0.17	76
7	+0.12	82
8	+0.30	78
9	+0.26	76
10	+0.28	76
11	+0.58	74
$Fe(C_5H_5)_2$	+0.44	72
$Fe(C_5Me_5)_2$	−0.12	82
$(C_5H_5)Fe(C_5H_4CH_2OH)$	+0.42	90
$(C_5H_5)Fe(C_5H_4CHO)$	+0.73	86

Qualitatively similar electrochemical behavior was exhibited by the structurally allied mononuclear complexes **6**–**11**. The relevant redox potentials are compiled in Table I.

As seen in Figure 2, the dimeric ether **12** undergoes two virtually overlapping, but distinguishable, one-electron oxidations ($E^{\circ\prime}_{(0/+)} \approx +0.25$ V; $E^{\circ\prime}_{(+/2+)} \approx +0.32$ V). Dinuclear ferrocenes in which the two subunits are electronically interacting are recognized to exhibit separate one-electron oxidations, while noncommunicating halves give rise to a single stepped two-electron oxidation. In the actual case of **12**, an intramolecular interaction between the two sandwich units appears to operate, although to a lesser extent.[22] The possibility of induction by means of heteroatom polarizability[23] cannot be ruled out.

In this connection, the data presented in Table I reflect some interesting electronic effects. It can be expected that fusion of a cyclopentadienide subunit to bicyclic frameworks will cause

(16) Freyberg, D. P.; Robbins, J. L.; Raymond, K. N.; Smart, J. C. *J. Am. Chem. Soc.* **1979**, *101*, 892.
(17) Miller, J. S.; Calabrese, J. C.; Rommelmann, H.; Chittipedi, S. R.; Zhang, J. H.; Reiff, W. M.; Epstein, A. J. *J. Am. Chem. Soc.* **1987**, *109*, 769.
(18) (a) Schumann, H.; Janiak, C.; Köhn, R. D.; Loebel, J.; Dietrich, A. *J. Organomet. Chem.* **1989**, *365*, 137. (b) Rausch, M. D.; Tsai, W.-M.; Chamgers, J. W.; Rogers, R. D.; Alt, H. G. *Organometallics* **1989**, *8*, 816.
(19) Zanello, P.; Cinquantini, A.; Mangani, S.; Opromolla, G.; Pardi, L.; Janiak, C.; Rausch, M. D. Submitted for publication.
(20) Brown, E. R.; Sandifer, J. R. In *Physical Methods of Chemistry. Electrochemical Methods;* Rossiter, B. W., Hamilton, J. F., Eds; Wiley: New York, 1986; Vol. 2, Chapter 4.
(21) Zanello, P. In *Stereochemistry of Organometallic and Inorganic Compounds*; Bernal, I., Ed.; Elsevier: Amsterdam, Vol. 4, 1990, p 181.

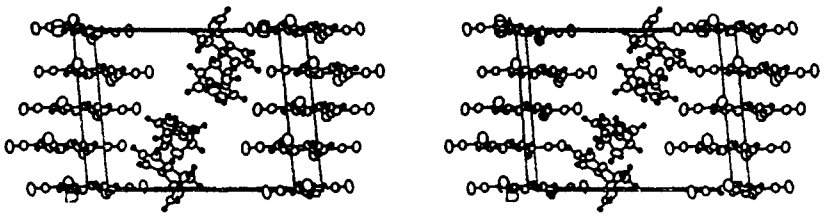

Figure 4. Unit cell of **5**·2TCNQ viewed down the *a* axis in stereo, with the *b* axis vertical and the *c* axis horizontal.

the oxidation of iron(II) to be more accessible than that of the parent ferrocene molecule. The oxidation potentials of **5–7**, when viewed comparatively, show the anion of **3** to be somewhat more electron-donating than the anion of **1**. The latter, in turn, is slightly more electron-donating than the anion of **2**. Further, higher shifts in oxidation potentials are brought on by the presence of the CHO and CH_2OH functions and not from the differing nature of the fused rings. Finally, the difference in redox potentials between **8** and **9** distinguishes electronic and steric contributions. Electron donation from the exo surface of the isodicyclopentadienide ligand is less than that stemming from the endo surface.

Independent confirmation of the higher electron-donating ability of **8**, **9**, and their analogues with respect to the ferrocenyl system comes from comparison of the potential of the two-electron oxidation of **12** (averaged value: +0.28 V) with that of $(C_5H_5)Fe(C_5H_4CH_2)O(CH_2C_5H_4)Fe(C_5H_5)$ (+0.56 V).[24]

Preparation of 5–7 and X-ray Crystallography of 5·2TCNQ. Ferrocenes **5** and **6** have been prepared by combining the appropriate cyclopentadienide anion with $FeCl_2$ in THF at various temperatures to control π-facial selectivity.[4,5,7,25] Recent modifications in their synthesis, as described in the Experimental Section, allow for easier isolation. The pinane-fused example **7** was comparably prepared by deprotonating **3** to generate its lithium salt and condensing of the latter with $FeCl_2$ in THF at −78 °C. Complexes **7** and **13** were obtained in a ratio of 3:1.

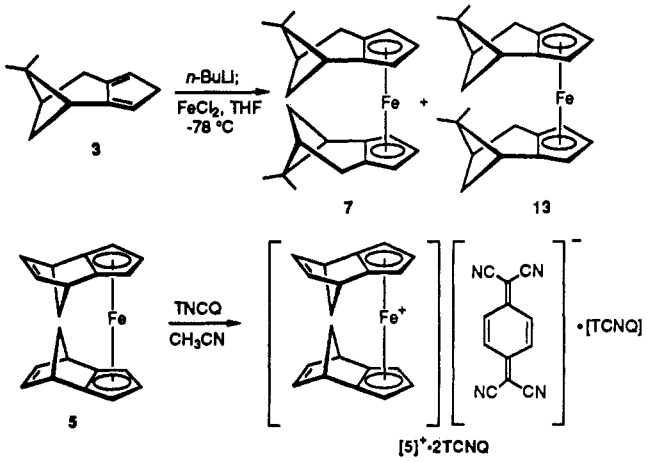

The oxidation of **5** was performed with TCNQ in acetonitrile solution.[26,27] The oxidation of Fe(II) to Fe(III) was easily recognized by the significant color change of the reaction mixture from yellow to purple black.

Table II. Crystal Details for $[5]^+$

formula	$Fe_1C_{44}H_{26}N_8$
fw	722.59
space group	$P\bar{1}$
a, Å	8.014(2)
b, Å	13.192(2)
c, Å	16.752(2)
α, deg	84.93(1)
β, deg	79.46(2)
γ, deg	79.11(2)
vol, Å^3	1707(1)
Z	2
density(calc), g/cm^3	1.41
cryst size, mm	0.12 × 0.35 × 0.46
radiation	Mo Kα with graphite monochromator
linear abs coeff, cm^{-1}	4.84
transm factors	0.92–1.00
temp, °C	23 °C
2θ limits, deg	$4 \le 2\theta \le 55$
scan speed, deg/min	4 (in ω with max of four scans per reflcn)
Bkg time/scan time	0.5
scan range, deg	$(1.15 + 0.35 \tan\theta)$ in ω
data collcd	$+h,\pm k,\pm l$
scan type	ω–2θ
no. of unique data	7848
no. of unique data, with $F_o^2 > 3\sigma(F_o^2)$	4632
final no. of variables	550
$R(F)^a$	0.037
$R_w(F)^b$	0.040
error in observn of unit weight, e	1.28

$^a R(F) = \sum||F_o| - |F_c||/\sum|F_o|$. $^b R_w(F) = [\sum w(|F_o| - |F_c|)^2/\sum wF_o^2]^{1/2}$ with $w = 1/\sigma^2(F_o)$.

The structural features of the resulting dark brown-purple plates were elucidated by X-ray crystallography using direct methods (SHELXS-86)[28] in $P\bar{1}$ (Table II, Figure 3). The asymmetric unit consists of one iron complex, one whole TCNQ molecule in a general position (TCNQ(3)), and two half-molecules of TCNQ with each situated about a different inversion center (TCNQ(1) and TCNQ(2)). The unit cell contains two iron complexes and four TCNQ molecules (Figure 4). The TCNQ molecules stack in columns which are parallel to the *b* axis direction. TCNQ(1) and TCNQ(2) are oriented in the same manner and are related by a shift of $^1/_2$ along the *b* axis. They are separated by TCNQ(3), which as seen in Figure 5 has the same orientation as TCNQ(1) or TCNQ(2), but is shifted in the *ac* plane. The stacking is diagrammed in Figure 6, where B (TCNQ(3)) is related to B′ by the crystallographic inversion center at $y = {}^1/_2$. TCNQ(1) and TCNQ(2) are not related by any crystallographic inversion center; since they are superimposable by a shift of $^1/_2$ in *y*, both are designated by "A" in Figure 6. Within each stack the molecules are equally spaced, as measured by the distance between least-squares planes for the benzene portions of adjacent TCNQ

(22) A reviewer requested that we compare the i_p(anodic)/c parameter for the oxidation processes of **5** and **12** illustrated in Figures 1 and 2, respectively, in order to assess better the two-electron oxidation of **12**. Since the Randles–Sevcik equation indicates dependence upon the diffusion coefficient D, and **5** and **12** certainly have different diffusion coefficients, we expect ratios of 0.35, 0.50, 0.61, and 0.71 for $D_5 = D_{12}$, $D_5 = 2D_{12}$, $D_5 = 3D_{12}$, and $D_5 = 4D_{12}$, respectively. Experimentally, we find a ratio of 0.65.

(23) O'Connor Salazar, D. C.; Cowan, D. O. *J. Organomet. Chem.* **1991**, *408*, 227.
(24) Silva, E. N. P. R. A.; Pombeiro, A. J. L.; Frausto da Silva, J. J. R.; Herrmann, R.; Deus, N.; Castilho, T. J.; Silva, M. F. C. G. *J. Organomet. Chem.* **1991**, *421*, 75.
(25) Bhide, V.; Rinaldi, P.; Farona, M. *J. Organomet. Chem.* **1989**, *376*, 91.
(26) Reis, A. H.; Preston, L. D.; Williams, J. M.; Peterson, S. W.; Candela, G. A.; Swartzendruber, L. J.; Miller, J. S. *J. Am. Chem. Soc.* **1979**, *101*, 2756.
(27) Deeming, A. J. In *Comprehensive Organometallic Chemistry*, Wilkinson, G., Ed.; Pergamon: Oxford, England, 1982; Vol. 4, pp 475–482.
(28) SHELXS-86, Sheldrick, G. M. In *Crystallographic Computing 3*, Sheldrick, G. M., Kruger, C., Goddard, R., Eds.; Oxford University Press: London, 1985; pp 175–189.

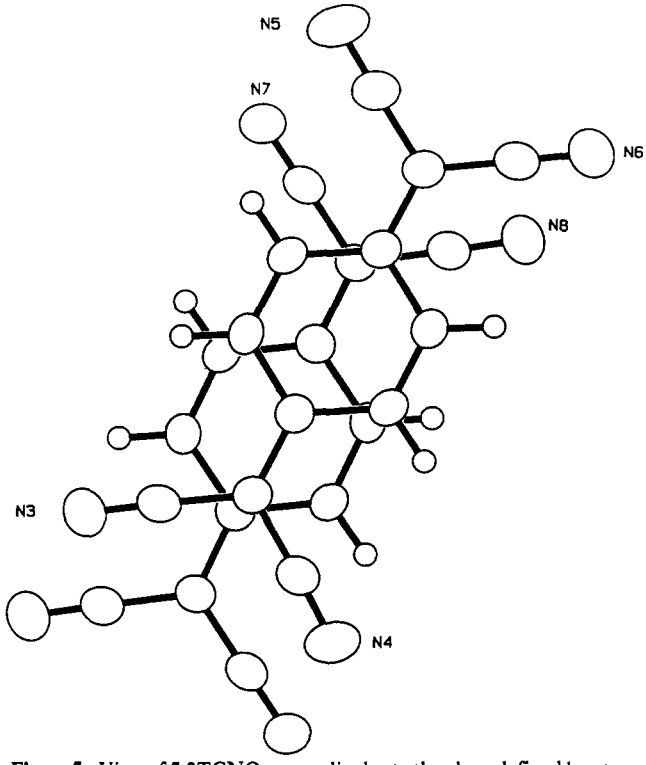

Figure 5. View of **5**·2TCNQ perpendicular to the plane defined by atoms C17–C18–C19 that shows the offset of TCNQ(1) (contains N7 and N8) with respect to TCNQ(3) (contains N3, N4, N5, N6).

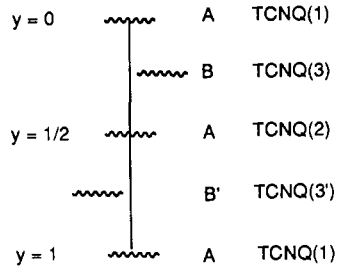

Figure 6. Stacking of the TCNQ molecules in **5**·2TCNQ.

molecules. The distance between TCNQ(1) and TCNQ(3) is 3.30 Å; the distance between TCNQ(3) and TCNQ(2) is 3.29 Å.

The charge associated with a TCNQ molecule has been correlated with the bond length differences $(b - c)$ and $(c - d)$, where b, c, and d are defined as follows:[29]

For a neutral TCNQ molecule, the differences $(b - c)$ and $(c - d)$ are +0.069 and −0.062 Å, respectively. For $TCNQ^-$, these values are 0 Å. The bond length differences and corresponding average charges for each TCNQ molecule are shown in Table III. The range of average charges observed for this structure (0.29–0.58 e) indicates that a full minus charge is not associated with any one of the TCNQ molecules.

Comparative Structural Analysis of 5 and [5]$^+$. The X-ray crystal structure of metallocene **5** has been reported earlier.[5] Since the molecules of $[5]^+$ find themselves located between the columns of TCNQ molecules and not otherwise perturbed by them (Figure 4), direct comparison of the neutral and charged species appeared reasonable. As seen in Table IV, the Fe–C and Fe–ring centroid

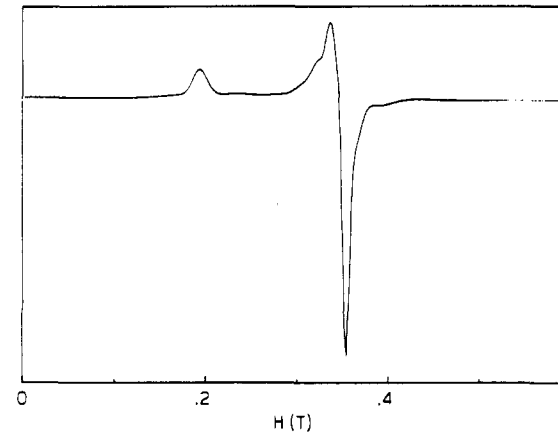

Figure 7. X-Band EPR spectrum of polycrystalline $[5]^+$ recorded at 4.2 K.

Table III. Average Charge for Each TCNQ Molecule in the Unit Cell of **5**·TCNQ

	$(b - c)$, Å	$(c - d)$, Å	av charge, e
TCNQ(1)	0.050, 0.048	−0.046, −0.042	0.29
TCNQ(2)	0.035, 0.041	−0.037, −0.041	0.41
TCNQ(3)	0.027, 0.034 0.029, 0.034	−0.031, −0.023 −0.022, −0.020	0.58

distances in $[5]^+$ are significantly longer than the same distances in **5**, whereas the C–C distances in the cyclopentadienyl rings remain almost unaltered. These features are typical of ferricinium and ferrocene systems.[10-19] Yet the intramolecular distance between the bridgehead carbons is shorter in $[5]^+$ at 3.881(5)Å (C(10A)---C(10B)) than in **5** at 4.287(2) Å (C(10)---C(20)). A consideration of comparable torsion angles shows that the Cp rings are more nearly eclipsed in **5** (torsion angle for C14–C15–C21–C25 = 3.3°) than in $[5]^+$ (torsion angle for C1B–C5B–C1A–C2A = 14.6°). This larger torsion angle in $[5]^+$ results in the shorter distance between the bridgehead carbon atoms. It is surprising that these carbon atoms have moved closer together instead of farther apart.

Both structures exhibit a small dihedral angle between the least-squares plane of a Cp ring and an adjacent four-atom fragment. For example, in **5** this angle is 10° for the best planes through C11–C12–C13–C14–C15 and C16–C15–C11–C19. The two carbon atoms bonded to the Cp ring in both structures are slightly displaced from the best plane through this ring and this displacement is always in the direction away from the Fe atom. The tricyclo[5.2.1.$0^{2,6}$]deca-2,5,8-trien-6-yl ligands have essentially the same geometry in both structures.

Electron Paramagnetic Resonance Studies. X-band EPR spectra of polycrystalline samples of the monocations $[5]^+$–$[11]^+$, obtained by exhaustive one-electron oxidation of the corresponding neutral congeners, were recorded at 4.2 K. The spectrum of $[5]^+$ displayed in Figure 7 is typical for these complexes.

The axial-type adsorption pattern with $g_\parallel = 3.67$ and $g_\perp = 1.90$ is characteristic of a ferrocenium ion in which the electron is removed from the iron center.[30] As usual, these species present fast spin-lattice relaxation, which makes them detectable only at liquid-helium temperature. The large axial anisotropy is responsible for orientation effects in the powder sample, which are observable as the weak features between 0.18 and 0.3 T.

Qualitatively similar spectra were obtained for $[6]^+$, $[7]^+$, $[8]^+$ and $[10]^+$, despite the existence of more effective orientation influences. In the case of $[9]^+$, these contributions are so pronounced that the relevant spectrum consists of a broad band ranging from 0.05 to 0.6 T and the extraction of the g parameters was not possible.

(29) Flandrois, S.; Chasseau, D. *Acta Crystallogr.* **1977**, *B33*, 2744.

(30) Duggan, D. M.; Hendrickson, D. N. *Inorg. Chem.* **1975**,*14*, 955.

Table IV. Geometrical Parameters for **5** and $[5]^+$ [a]

		5		$[5]^+$
range of Fe–C dist where C is in a Cp ring		2.026–2.065		2.046–2.140
Fe···RCA[b]		1.659(1)		1.720(3)
Fe···RCB		1.658(1)		1.719(3)
RCA···RCB		3.316(2)		3.439(4)
RCA-Fe-RCB		177.4(1)		177.4(2)
C–C dist in Cp rings		1.408–1.431		1.398–1.423
C(10A)···C(10B) or C(10)···C(20)		4.287(2)		3.881(5)
dihedral angle between Cp rings		3.7		7.1
dihedral angle between Cp ring and four atom "best" plane	10.0	C11–C12–C13–C14–C15 + C16–C15–C11–C19	7.2	C1A–C2A–C3A–C4A–C5A + C5A–C6A–C9A–C1A
	9.3	C21–C22–C23–C24–C25 + C26–C25–C21–C29	6.4	C1B–C2B–C3B–C4B–C5B + C5B–C6B–C9B–C1B

[a] Distances are in Å and angles are in degrees. [b] RCA is the ring centroid for C11–C12–C13–C14–C15 of **5** or the ring centroid for C1A–C2A–C3A–C4A–C5A of **5**·2TCNQ. RCB is the ring centroid for C21–C22–C23–C24–C25 of **5** or the ring centroid for C1B–C2B–C3B–C4B–C5B of **5**·2TCNQ.

Table V. EPR Data for the Polycrystalline Powder Samples of the Monocations Studied at 4.2 K

sample	$g_\parallel$	$g_\perp$	Δg
[5]+	3.67	1.90	1.77
[6]+	3.73	1.81	1.92
[7]+	3.23	1.99	1.24
[8]+	3.55	1.81	1.74
[10]+	3.67	1.84	1.83

Finally, the spectrum of $[11]^+$ shows several features which are presumably attributable to the presence of iron(III) byproducts arising from slight decomposition of the electrogenerated monocation. These impurities give rise to a band centered at $g = 4.3$, which hides the $g_\parallel$ region of the ferrocenium ion having $g_\perp = 2.0$.

Table V summarizes the EPR spectral features of the collective monocations. The polycrystalline nature of the samples renders impossible a more accurate analysis, due in large part to the existence of orientation effects.

The current interpretation accorded to the EPR spectra of ferrocenium cations[30–32] has the anisotropy of the spectrum, as measured by the $\Delta g = g_\parallel - g_\perp$, dependent upon the extent of the low-symmetry crystal field distortions (lower than D_5). When no low symmetry component of the crystal field is present $g_\parallel = 6$ and $g_\perp = 0$; increasing distortions make both $g_\parallel$ and $g_\perp$ values approach the isotropic $g = 2$ value. A comparison of the EPR parameters of the present ferrocenium complexes with existing literature values[30–32] shows that the extent of symmetry distortion falls into an already observed Δg range. In particular, a comparison between the spectrum of $[5]^+$ with that of 1,1′-(propane-1,3-diyl)ferrocenium iodide[32] seems useful. In the crystal structure of $[5]^+$ the dihedral angle between the cyclopentadienyl rings is 7.1° while for 1,1′-(propane-1,3-diyl)ferrocenium iodide it is 8.2° and 13.4° for the two different asymmetric units, respectively. The observed EPR powder spectrum of the latter compound, recorded at 77 K, shows a broad feature at $g = 2$, thus confirming the influence of low symmetry distortions in determining the anisotropy of EPR spectra in ferrocenium species. In this light, the fact that $[7]^+$ exhibits the lowest Δg value is likely indicative of the relatively higher distortions caused by the two sterically encumbering pinane-fused facing rings.

Conclusions. The electrochemical behavior of a series of ferrocene molecules in which the cyclopentadienyl rings are fused with pinane or norbornane rings show that these systems reversibly lose one electron more easily than unsubstituted ferrocene. To some extent, the removal of the electron is also affected by the coordination mode of such fragments above or below the plane of the cyclopentadienyl rings. In agreement with the near electrochemical reversibility of the oxidation process of bis(η^5-tricyclo-[5.2.1.0^{2,6}]deca-2,5,8-trien-6-yl)iron(II) (**5**), the crystal structures of the iron (II)/iron(III) congeners **5**/$[5]^+$ show that the one-electron removal is accompanied by minor stereochemical reorganizations, which have been analyzed in detail.

(31) Prins, R. *Mol. Phys.* **1970**, *19*, 603.
(32) Dong, T. Y.; Hwang, M. Y.; Lee, T. Y.; Tseng, L. H.; Peng, S. M.; Lee, G. H. *J. Organomet. Chem.* **1991**, *414*, 603.

Experimental Section

Materials and apparatus for the electrochemical measurements have been described elsewhere.[1] Potential values are referenced to the saturated calomel electrode (SCE). A rough evaluation of the formal electrode potentials of the two consecutive one-electron removals from **12** was carried out by assuming that each of the two redox couples displays a peak-to-peak separation similar to that of the corresponding mononuclear complex **10**.

Electron paramagnetic resonance spectra were recorded with a Varian E9 spectrometer operating at the X-band frequency (9.24 GHz). Liquid-helium temperature spectra were recorded with the aid of an Oxford Instruments ESR9 liquid-helium continuous-flow cryostat. All reactions were performed under argon using standard Schlenk-line techniques. Solvents were dried and distilled prior to use.

Bis(η^5-*exo*-tricyclo[5.2.1.0^{2,6}]deca-2,5,8-trien-6-yl)iron (5). The lithium salt (1.00 g, 7.35 mmol) generated from tricyclo[5.2.1.0^{2,6}]deca-2,5,8-triene was dissolved in THF (30 mL) and added slowly via cannula to $FeCl_2$ (460 mg, 3.6 mmol) slurried in 30 mL of THF at room temperature. The reaction mixture turned brown as addition took place. After 24 h, the solvent was removed under vacuum to leave a brown residue, which was extracted with several portions of benzene until the extractions were colorless. The combined benzene fractions were filtered through a pad of Celite and concentrated to leave an orange oil. Hexane was added to redissolve the oil. Crystallization at −20 °C afforded complex **5** (593 mg, 52%): mp 162–164 °C; ^{1}H NMR (300 MHz, C_6D_6) δ 6.32 (t, J = 1.7 Hz, 4 H), 3.93 (t, J = 2.0 Hz, 4 H), 3.77 (d, J = 2.0 Hz, 2 H), 3.27 (t, J = 1.6 Hz, 4 H), 2.93 (d, J = 6.6 Hz, 2 H), 2.19 (d, J = 6.6 Hz, 2 H); ^{13}C NMR (75 MHz, C_6D_6) δ 140.93, 104.85, 67.90, 65.84, 61.76, 43.77.

Analytical data have been reported previously.[5]

Bis(η^5-*exo*-tricyclo[5.2.1.0^{2,6}]deca-2,5-dien-6-yl)iron (6). Isodicyclopentadienyllithium (519 mg, 4.2 mmol) and 30 mL of THF were combined and added dropwise via cannula over 30 min to a slurry of iron(II) chloride (262 mg, 2.1 mmol) in 30 mL of THF at 25 °C. As addition took place, the slurry changed in color from peach-tan to brown. The reaction mixture was stirred for 24 h before the solvent was removed in vacuo. The brown residue was leached with several portions of benzene. Inorganic solids were removed by filtration through a pad of Celite, leaving a bright orange solution. The filtrate was concentrated to leave an orange-red crystalline solid. Sublimation (95–100 °C, 0.003 Torr) afforded 599 mg (91%) of a yellow solid consisting of three isomeric products indicated by ^{1}H NMR. Complex **6**, the major component, was isolated by recrystallization from hexane at −20 °C, to give 375 mg (57%) of pure **6**: mp 168–169 °C; ^{1}H NMR (300 MHz, C_6D_6) δ 3.94 (d, J = 1.3 Hz,

2 H), 3.75 (d, J = 1.8 Hz, 4 H), 2.81 (br s, 4 H), 2.35 (dd, J = 4.0, 1.5 Hz, 2 H), 1.62 (d, J = 13.9 Hz, 4 H), 1.26 (d, J = 8.1 Hz, 2 H), 1.05 (dd, J = 7.1, 2.2 Hz, 4 H); ^{13}C NMR (75 MHz, C_6D_6) δ 97.94, 68.10, 59.54, 48.28, 38.00, 28.95.

Analytical data have been reported previously.[5]

Bis(η^5-[(1S,8R)-9,9-dimethyltricyclo[6.1.1.0^{2,6}]deca-2,5-dienyl])iron (7 and 13). Into a round-bottomed flask with sidearm was weighed the lithium salt of **3** (2.00 g, 12.0 mmol), and the solid was dissolved in 40 mL of THF. $FeCl_2$ (744 mg, 5.87 mmol) was weighed into a second flask, slurried in 40 mL of THF, cooled to −78 °C, and treated dropwise via cannula with the anion solution. The mixture was kept at −78 °C for 1 h before being allowed to warm to room temperature. After 10 h, the solvent was removed in vacuo to leave a brown residue. Benzene (approximately 100 mL) was added in portions to loosen the residue, and the slurry was passed through a pad of Celite, giving an orange filtrate. The filtrate was concentrated leaving an orange oil, TLC analysis of which indicated the presence of two compounds. MPLC purification of the oil afforded **7** and **13**, the latter decomposing rapidly after isolation. Integration of the MPLC trace indicated the exo,exo to exo,endo ratio to be 3:1. No endo,endo isomer was seen spectroscopically. Isolated after recrystallization was 1.46 g (66%) of **7** and 70 mg (3%) of **13**.

For **7**: mp 89–91 °C; ^{1}H NMR (300 MHz, C_6D_6) δ 3.95 (br s, 2 H), 3.79 (br d, J = 5.8 Hz, 4 H), 2.72 (br d, J = 17.7 Hz, 2 H), 2.65 (dt, J = 8.9, 5.9 Hz, 2 H), 2.37 (t, J = 5.5 Hz, 2 H), 2.35 (dt, J = 12.5, 1.8 Hz, 4 H), 2.03 (br m, J = 2.7 Hz, 2 H), 1.28 (s, 6 H), 0.57 (s, 6 H); ^{13}C NMR (75 MHz, C_6D_6) δ 98.42, 81.38, 67.39, 65.37, 65.21, 42.40, 41.79, 41.53, 36.09, 27.06, 26.96, 21.49; MS m/z [M$^+$] calcd for $C_{24}H_{30}Fe$, 374.1697, m/z obsd, 374.1696; $[\alpha]_D^{20}$ −554.2° (c 0.6 hexane).

For **13**: mp 46–48 °C; ^{1}H NMR (300 MHz, C_6D_6) δ 3.99 (t, J = 2.0 Hz, 1 H), 3.95 (br s, 1 H), 3.88 (br s, 1 H), 3.78 (br s, 1 H), 3.71 (d, J = 0.9 Hz, 1 H), 3.63 (br s, 1 H), 2.79 (dd, J = 15.5, 2.3 Hz, 2 H), 2.72 (t, J = 6.1 Hz, 1 H), 2.66 (dd, J = 15.7, 1.6 Hz, 1 H), 2.38 (m, 4 H), 2.30 (dt, J = 13.8, 3.6 Hz, 1 H), 2.04 (br s, 1 H), 1.97 (dd, J = 3.3, 1.4 Hz, 1 H), 1.63 (s, 3 H), 1.29 (s, 3 H), 1.27 (s, 3 H), 0.75 (dd, J = 8.7 1.9 Hz, 1 H), 0.56 (s, 3 H); ^{13}C NMR (75 MHz, C_6D_6) δ 98.37, 97.53, 81.98, 81.53, 70.21, 69.49, 65.35, 65.02, 63.67, 61.84, 42.30, 41.49, 41.40, 40.90, 36.13, 35.85, 30.16, 28.28, 27.80, 27.15, 27.10, 27.04, 23.68, 21.49; MS m/z [M$^+$] calcd for $C_{24}H_{30}Fe$, 374.1697, m/z obsd, 374.1682; $[\alpha_D^{20}]$ −350° (c 0.3, hexane).

Anal. Calcd for $C_{24}H_{30}Fe$: C, 77.00; H, 8.08 Found: C, 76.57; H, 8.28.

Oxidation of 5. Complex **5** (50.0 mg, 0.16 mmol) was dissolved in 5 mL of dry acetonitrile. In another flask was placed 7,7,8,8-tetracyano-p-quinodimethane (32.5 mg, 0.16 mmol), 5 mL of benzene, and 5 mL of CH_2Cl_2. This mixture was added to the orange ferrocene solution via cannula. An additional 3 mL of CH_2Cl_2 was added to dissolve the remaining solids. Upon addition, the mixture turned green. The solvent was removed in vacuo, leaving a gray-green solid, which was dissolved in a minimal amount of acetonitrile and allowed to stand at room temperature for 10 h. A dark shiny purple crystalline solid formed and was collected. After washing with pentane, there was isolated 47.3 mg (41%) of [**5**]$^+$·2TCNQ, mp >250 °C.

Anal. Calcd for $C_{44}H_{26}N_8Fe$: C, 73.14; H, 3.63 Found: C, 72.59; H, 3.64.

X-ray Crystal Structure Analysis of 5-TCNQ. The data collection crystal was cleanly cut from a larger plate. Examination of the diffraction pattern on a Rigaku AFC5S diffractometer indicated a triclinic crystal system; the space group possibilities are restricted to $P1$ or $P\bar{1}$. The unit cell constants are based on a least-squares fit of the diffractometer setting angles for 25 reflections in the 2θ range 23–30° with Mo Kα radiation (λ(K$\bar{\alpha}$) = 0.710 73 Å).

Intensities were measured by the ω–2θ scan method. Six standard reflections were measured after every 150 reflections and indicated that the crystal was stable throughout data collection. The structure was solved in $P\bar{1}$ with the direct methods procedure of SHELXS-86.[28] All full-matrix least-squares refinements were done with the TEXSAN package of crystallographic programs.[33] The data set was corrected for absorption by the ψ scan method.[34] After the anisotropic stage of refinement had been reached, all 26 hydrogen atoms were located on a difference electron density map. The hydrogen atoms on the iron complex were refined isotropically. The hydrogen atoms of the TCNQ molecules were included in the model as fixed contributions in calculated positions with C–H = 0.98 Å and $B_H = 1.2B_{eq}$ (attached carbon atom). The final refinement cycle was based on the 4632 intensities with $F_o^2 > 3\sigma(F_o^2)$ and 550 variables and yielded agreement factors of $R(F)$ = 0.037 and $R_w(F)$ = 0.040. The final difference electron density map contains maximum and minimum peak heights of +0.18 and −0.30 e/Å^3. Scattering factors were obtained from the usual sources.[35]

Acknowledgment. The Ohio State group is grateful to the National Science Foundation for financial support. M.R.S. thanks the U.S. Department of Education for National Needs Fellowships and the Amoco Foundation for a fellowship.

Supplementary Material Available: Tables giving bond distances, bond angles, hydrogen-bonding distances, least-squares planes, positional parameters for non-hydrogen atoms, hydrogen atom parameters, and anisotropic thermal parameters (14 pages). Ordering information is given on any current masthead page.

(33) TEXSAN, Single Crystal Structure Analysis Software, Version 5.0. Molecular Structure Corp., The Woodlands, TX, 1989.
(34) North, A. C. T.; Phillips, D. C.; Mathews, F. S. *Acta Crystallogr.* **1968**, *A24*, 351.
(35) Scattering factors for the non-hydrogen atoms, including terms for anomalous dispersion, are from: *International Tables for X-ray Crystallography*, Kynoch Press: Birmingham, England, 1974, Vol. IV, pp 71 and 148. The scattering factor for the hydrogen atom is from: Stewart, R. F.; Davidson, E. R.; Simpson, W. T. *J. Chem. Phys.* **1965**, *42*, 3175.